Semesta Teknika
Vol. 27, No. 1, 55-65, Mei 2024
DOI: https://doi.org/10.18196/st.v27i1.21753
© The Author (s) 2024

Thermal Stratification Characteristics of Storage Tanks on Solar Water Heater Inserted with Latent Heat Material

Muhammad Nadjib*, Wahyudi, Tito Hadji Agung Santosa, Yaafi Hidayat
Department of Mechanical Engineering, Faculty of Engineering, Universitas Muhammadiyah Yogyakarta

Jl. Brawijaya, Tamantirto, Kasihan, Bantul, Yogyakarta, Indonesia

* Corresponding author email: nadjibar@umy.ac.id

Check for updates

Keywords:
Capsule; heat storage; phase change material; solar water heater; thermal stratification

Abstract
As a latent heat medium, phase change material (PCM) can be applied to heat storage for solar water heaters (SWH). The method used to place PCM is to put it in a capsule. Thermal stratification is critical in generating SWH thermal efficiency. Installation of horizontal capsules in the tank has no known effect on thermal stratification. This paper aims to study the thermal stratification in active-type SWH incorporating PCM. A cylindrical capsule containing the PCM was placed inside the tank. The thermocouple was installed on both the water and PCM sides. The charging process was conducted indoors, and the water flow rate varied from 1, 2, and 3 LPM. Water temperature data for each variation was analyzed to evaluate the thermal stratification. Richardson number analysis proved that thermal stratification was formed in all water flow rates. It was found that a low water flow rate results in high thermal stratification.

INTRODUCTION

Energy has a vital role in human life. Energy is helpful for human welfare, including economic development and encouraging a country's economic growth (Shahsavari & Akbari, 2018). Energy is grouped into fossil and renewable energy based on its origin. Fossil energy dominates energy use globally at 84.7% (Ostadzadeh et al., 2023). Alternatively, there is considerable uncertainty surrounding the prospects of the global fossil fuel sector in the long term. This uncertainty comes from physical quantity and the available resources that can be extracted (Bauer et al., 2016). Therefore, diversification of energy sources must be encouraged to reduce fossil energy consumption. Renewable energy represents a viable alternative, with the sun as one of its sources. The sun is the primary energy source on earth (Kabir et al., 2018). The annual solar radiation received by the earth's surface reaches 3.4 x 10^6 exajoules (World Energy Council, 2013). Solar energy is environmentally friendly and will not run out if there is life. Solar energy applications are grouped into two conversion systems: electrical and thermal energy. Photovoltaic technology is an example of an application for converting solar electromagnetic energy to electrical energy. Solar power can be transformed into thermal energy to heat various heating systems. Solar water heater (SWH) is equipment used to heat water using energy from the sun. The energy conversion process in SWH is simple because it comes directly from solar energy. Hot water is needed for domestic, commercial, or industrial human activities (Singh et al., 2020). Based on its operation, SWH is classified into passive and active types (Jamar et al., 2016). The heat transfer fluid (HTF) flow in passive type SWH occurs naturally due to buoyancy force. The HTF in the active type SWH is driven forcefully by a pump. The SWH application provides tangible benefits, namely that it can reduce fossil energy consumption (Uctug & Azapagic, 2018). According to Kushwaha et al. (2023), SWH stands out as among the most employed solar energy applications at the household level.

Thermal energy storage can be done using three methods: chemical energy, sensible heat (SH), and latent heat (LH) (Anisur et al., 2013). The heat of chemical energy relates to the energy required or released during a reaction. SH is a heat storage involving changes in material temperature. Within the LH system, thermal energy is stored through the process of a material undergoing a phase transition, such as freezing or melting (Khare et

al., 2013), or is called phase change material (PCM). In conventional SWH, water as an SH material stores thermal energy. Nevertheless, Fang et al. (2018) argue that water use is weak: low energy density. Energy density is the amount of thermal energy contained in each volume of a substance. Substances with low energy density require sizeable thermal energy storage areas. The weakness of SH can be replaced with LH because it has high energy density and low-temperature changes during heat absorption and release (Patel & Namjoshi, 2018). Therefore, LH is suitable for application in solar energy equipment, including SWH (Kushwaha et al., 2023).

PCM is grouped into three types: salt hydrates, paraffin, and non-paraffin organic. Paraffin is an attractive material to apply because it is chemically stable and nontoxic and has a high latent heat (Murali et al., 2015). Paraffin is a hydrocarbon substance. Paraffin possesses nearly all the desired characteristics required for storage systems, apart from its relatively high thermal conductivity, as Fazilati and Alemrajabi (2013) noted. In the literature, researchers conducted studies on applying PCM to SWH. The presence of cylindrical capsules filled with paraffin wax within SWH tanks accelerates the rise in water temperature, particularly at elevated positions within the tank (Kanimozhi & Bapu, 2012). Combining PCM and graphite can reduce charging and discharging time (Shabtay & Black, 2014). Fukahori et al. (2016) examined the arrangement of capsules containing PCM and concluded that the presence of PCM could increase heat transfer in the SWH tank. Adding PCM to the tank can extend the hot water usage time (Sobhansarbandi et al., 2017). The influence of solar radiation fluctuations can be reduced by adding PCM in storage (Wu et al., 2018). According to Nazir et al. (2019), tanks containing PCM have higher heat absorption than tanks containing only water. The configuration of PCM capsules within the tank effectively operates as a heat exchanger (Nadjib et al., 2020). The energy density of conventional SWH can be increased by inserting a cylindrical capsule in the tank (Koželj et al., 2021). Incorporating PCM in SWH increases hot water production (Naveenkumar et al., 2022). The findings presented in the study indicate that employing PCM can enhance thermal behavior of SWH systems.

Thermal stratification is a critical factor in SWH tanks. Thermal stratification in water-filled thermal energy storage (TES) tanks is characterized by forming distinct horizontal layers with varying temperatures, with the warmer layer at the top (Chidambaram et al., 2011). The presence of thermal stratification suggests an ongoing heat transfer process from the warmer to the more relaxed layer, contributing to the enhanced thermal efficiency of the SWH system (Pinel et al., 2011). Enhancing the thermal efficiency of a passive SWH system can be achieved by creating a temperature disparity between the inlet and outlet of the water tank (Dehghan & Barzegar, 2011). Consequently, hot water enters the tank at the top and comes out at the bottom (Chandra & Matuska, 2019). The enhanced thermal efficiency, as indicated by the findings of the three preceding authors, is attributed to the stratification process, which leads to a lower water temperature entering the collector, consequently diminishing convective heat loss and radiation to the surroundings. This phenomenon results in a heightened absorption of thermal energy by the collector. Several studies have analyzed the thermal stratification of PCM use in SWH. Fazilati and Alemrajabi (2013) stated that using PCM in tanks can maintain thermal stratification at the charging and discharging stages. Applying PCM to SWH can improve the tank's thermal performance by increasing the stratification rate, energy efficiency during charging, and thermal efficiency (Murali et al., 2015). Kumar et al. (2016) discovered that incorporating PCM capsules into the tank resulted in heightened thermal stratification due to the augmented temperature gap between the hot water inlet and the melting point of the PCM. Augmenting the quantity of PCM in the inlet region can lead to an elevation in the thermal stratification of the tank, even when the water flow rate remains constant (Huang et al., 2019). The formation of thermal stratification in TES tanks is primarily influenced by the water flow rate (Majumdar & Saha, 2019). Installing an equalizer at the tank inlet can improve the thermal stratification of tanks containing PCM and stabilize hot water output (Wang et al., 2020).

The SWH system involving PCM has a capsule arrangement in the tank. Encapsulation is a method for storing PCM with certain materials (Salunkhe & Shembekar, 2012). Using PCM modules is an auspicious way to produce hot water during discharge (Abokersh et al., 2018). The PCM capsule is cylindrical for horizontal SWH tanks, and several capsules are arranged parallel to the tank axis to form a heat exchanger (Nadjib et al., 2020). Based on previous studies on thermal stratification in SWH, no one has examined the characteristics of this parameter where PCM-filled capsules are employed horizontally within an active-type SWH tank. The arrangement of capsules is likely to affect the development of thermal stratification within the tank. This study

aims to examine the development of thermal stratification in an active-type SWH system utilizing a horizontally positioned tank and featuring a configuration of PCM capsules.

RESEARCH METHODS

Materials

This experiment combines water and PCM within SWH tanks to serve as thermal energy storage mediums. Water acts as HTF that circulates in the SWH system. The PCM used was paraffin wax RT55. Table 1 shows the technical specifications of RT55 paraffin wax type PCM.RT55.

Table 1. Technical specification of paraffin wax RT55 (Rubitherm Technologies GmbH, 2020)

Properties	Values
Melting temperature	51—57°C
Latent heat capacity	170 kJ/kg
Specific heat	2 kJ/kg.K
Solid density	0.88 kg/l
Liquid density	0.77 kg/l
Thermal conductivity (solid & liquid)	0.2 W/m.K
Expansion (volume)	14%
Flash point	>200°C
Maximum operation temperature	90°C

Experimental Setup

The experiment employs an active-type SWH system featuring a configuration illustrated in Figure 1. The primary elements of the setup include the TES tank, collector panel, solar simulator, pump, capsule configuration, and piping system. The piping arrangement comprises two lines: one for transporting hot water from the collector to the tank and the other for circulating return water from the tank back to the collector.

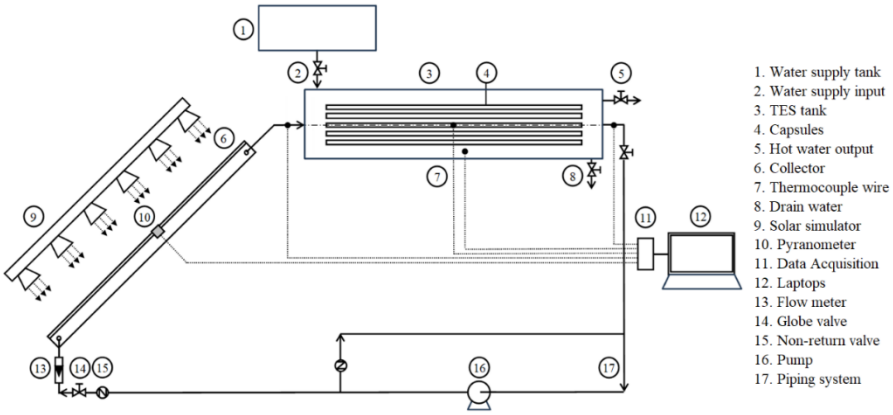

Figure 1. Scheme of experimental equipment

Experiments were carried out by varying the water flow rate. Under these conditions, outdoor experiments are impossible because the intensity of solar radiation fluctuates constantly. Therefore, the experiment was carried out indoors using a solar simulator as an energy source for the collector. The solar simulator employs a set of 24 halogen lamps, with each lamp having a power rating of 300 watts. The solar simulator was placed above the collector. The solar simulator and collector were set at a tilt angle of 15°. A flat plate-type collector, spanning 1.99 m^2 in surface area, was utilized in this experiment. This collector was linked to a TES tank holding a capacity of 60 liters. The tank placement position is horizontal. The TES tank contains 21 cylindrical capsules arranged according to the crushing type, where the central capsule axis of the capsule arrangement

coincides with the inlet water channel axis. The capsule was constructed from copper tubing measuring 100 cm long and having an external diameter of 1 inch. Each capsule was filled with 331.84 grams of paraffin wax. Twelve type K thermocouples were installed on the HTF side, while ten thermocouples are for PCM. Thermocouples for PCM were placed on the capsule axis with two each (T1 to T10). Thermocouples for HTF were installed between two capsules, with two pieces for each thermocouple height position (T11 to T22). The capsule arrangement and thermocouple installation location are presented in Figure 2.

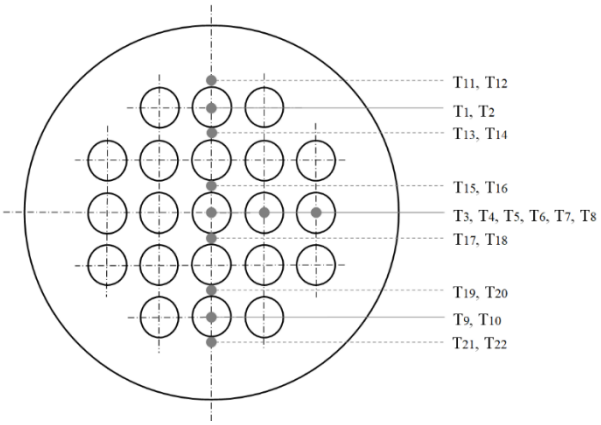

Figure 2. Capsules arrangement and thermocouple's location

The first step in the experiment is to set up the solar simulator to produce a heat flux of 1000 W/m^2. The device employed for measuring and capturing heat flux was a pyranometer sourced from the Hobo Weather Station, boasting an accuracy within ± 10 W/m^2 and a resolution of 1.25 W/m^2. These pyranometers were strategically positioned beneath the solar simulator at multiple locations. Before activating the light for 15 minutes and recording the heat flux, the voltage at each pyranometer's location is regulated by a voltage regulator, aligning the solar simulator's height to the collector. This experiment utilizes a voltage regulator capable of a maximum voltage and current of 250 V and 20 A, respectively. Following data collection, the recorded heat flux results are averaged based on the voltage data and the distance between the solar simulator and the collector at each pyranometer position. The voltage selection from the regulator and the distance between the solar simulator and the collector is meticulously undertaken to yield an averaged heat flux approximation nearing 1000 W/m^2. After the heat flux reaches 1000 W/m^2, the solar simulator is turned off and continued by filling the SWH system with water. The next step was to turn on the pump, so the HTF circulates in the SWH system. The pump in this experiment operates at 220 volts with an input power rating of 300 watts. This pump can achieve a maximum flow rate of 10 liters per minute and generate a maximum head of 33 m. The water flow rate was set at 1 LPM using a globe valve. If the flow conditions in the flow meter are stable, the solar simulator and data acquisition are activated. The flow meter employed was in-line, boasting a maximum flow rate of 7.5 liters per minute and exhibiting an accuracy level of ±5%. HTF and PCM temperature recording begins. Temperature data collection was facilitated by an AT4532 multi-channel temperature meter featuring 32 channels. It offers an accuracy of 0.2%+1°C and provides a resolution of 0.1°C. The SWH heating process was carried out for 160 minutes. The experimental procedure was repeated similarly for 2 and 3 LPM water flow rates.

The temperature data collected during the experiment was utilized to examine the thermal properties of the HTF and PCM during the charging process. The average temperature progression of HTF and PCM were analyzed from the initiation to the completion of charging. HTF and PCM temperature evolutions were also made for each thermocouple position height. The subsequent stage involves assessing the thermal layering of HTF within the tank during charging, employing the Richardson number (Ri). The Richardson number indicates the ratio of buoyancy force to mixing force and is defined as follows (Castell et al., 2010).

$$Ri = \frac{g.\beta.H.(T_{top} - T_{bottom})}{v_s^2} \quad (1)$$

$$v_s = \frac{Q}{\pi.r_s^2} \quad (2)$$

with g = acceleration of gravity (m^2/s), β = thermal expansion coefficient (1/°C), H = the tank height (m), T_{top} = temperature at the upper of the tank (°C), T_{bottom} = temperature at the lowest point of the tank (°C), v_s = average velocity of the water at the stratifier (m/s), Q = water flow rate (m^3/s), and r_s = stratifier radius (m).

Equation (1) clarifies that H denotes the height of the tank. In this experiment, a tank was employed in a horizontal orientation, ensuring that the tank's height corresponds to its diameter. Utilizing Equation (1) and Equation (2), a graph depicting the Richardson number during charging was plotted for the three different flow rate variations. The analysis focused on discerning the impact of flow rate on the thermal layering within the TES tank.

RESULTS AND DISCUSSION

HTF Average Temperature Evolution

The number of thermocouples that record HTF temperatures is 12 pieces (Figure 2). The average temperature of all thermocouples from the beginning to the end of charging forms the HTF evolution for the three variations in flow rate, as shown in Figure 3. The graph in Figure 3 was obtained for a heat flux of 1000 W/m^2 and 21 capsules.

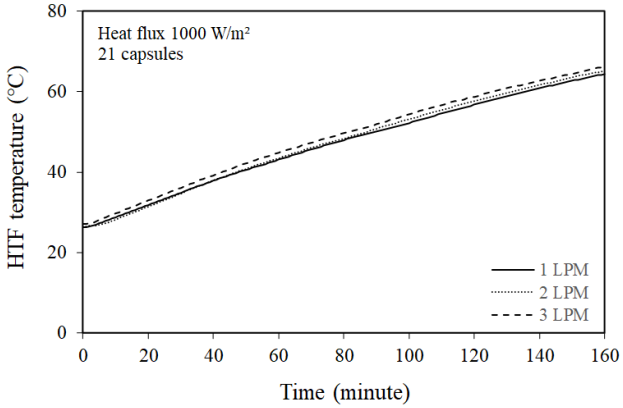

Figure 3. Evolution of average HTF temperature with variations in flow rate

Figure 3 illustrates a consistent rise in HTF temperature over time, regardless of variations in water flow rate. As the heating process extends, the collector accumulates more thermal energy, increasing hot water production. This hot water is then directed into the TES tank, initiating heat transfer due to the temperature disparity between the hot water and the tank's contents. Consequently, the water in the tank experiences a boost in thermal energy content, leading to a steady temperature elevation. The absence of fluctuations in temperature increase can be attributed to the consistent heat flux received by the collector.

According to the data presented in Figure 3, the initial and final temperatures of the HTF for water flow rates of 1, 2, and 3 LPM are as follows: 26.23°C and 64.38°C, 26.53°C and 65.19°C, and 27.09°C and 66.24°C, respectively. The temperature differentials observed during charging for water flow rates of 1, 2, and 3 LPM are 38.15°C, 38.66°C, and 39.14°C, respectively. The HTF heating rates for water flow rates of 1, 2, and 3 LPM are 0.238 °C/minute, 0.242 °C/minute, and 0.245 °C/minute, respectively. This heating rate denotes the temperature increase experienced by the HTF within the tank per minute. The data suggests that higher flow rates correspond to elevated HTF temperatures. These findings are consistent with prior research conclusions. Xiao and Zhang (2015) determined that increased water flow rates lead to faster charging due to the heightened temperature differential between the HTF and PCM. A higher HTF flow rate indicates a more significant mass flow rate, resulting in increased thermal energy extraction from the absorber plate at the collector, thereby yielding a higher collector exit temperature.

PCM Average Temperature Evolution

Figure 4 illustrates how the average temperature of the PCM in the TES tank changes as the water flow rate varies. The PCM's average temperature during the charging phase follows a pattern akin to that of the HTF's average temperature: as the charging duration increases, the PCM temperature steadily rises. This process initiates a rise in the tank's HTF temperature due to the infusion of hot water from the collector. As the HTF temperature elevates, the temperature gap with the PCM widens, facilitating heat transfer from the HTF to the PCM via the walls of the capsules. Heat transfer from the HTF to the PCM predominantly transpires through conduction since the PCM remains in its solid phase. The slow conduction of heat is attributed to the low thermal conductivity of the PCM, resulting in a gradual increase in PCM temperature at the outset of the charging process, as depicted in Figure 4. As the charging duration extends, the temperature contrast between the HTF and PCM widens, leading to a heightened influx of thermal energy absorbed by the PCM. Subsequently, the heat transfer mechanism transitions from conduction to natural convection. The onset of PCM melting, induced by PCM movement, amplifies the natural convection process, leading to a swift escalation in PCM temperature.

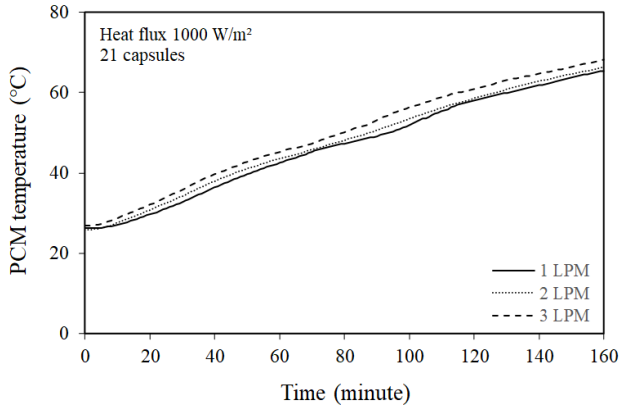

Figure 4. Evolution of average PCM temperature with variations in flow rate

According to the information provided in Figure 4, the initial and final PCM temperatures during the charging process vary for water flow rates of 1, 2, and 3 LPM. They are as follows: 26.17°C and 65.43°C, 25.89°C and 66.32°C, and 26.88°C and 68.18°C, respectively. The disparity in PCM temperature between the final and initial states for water flow rates of 1, 2, and 3 LPM stands at 39.26°C, 40.45°C, and 41.29°C, correspondingly. Additionally, the rate of PCM heating for water flow rates of 1, 2, and 3 LPM is calculated as 0.245°C/minute, 0.253°C/minute, and 0.258°C/minute, respectively. This data underscores that higher water flow rates correlate with increased thermal energy within the PCM. A high PCM temperature indicates a high thermal energy content. The study's results by Chopra et al. (2020) show suitability with this research. Authors state that in evacuated tube-type SWHs containing PCM, the water flow rate significantly influences the PCM charging process. In other words, water with a high flow rate produces a high PCM temperature.

Figure 4 also provides information about the PCM melting process. However, PCM phase changes occur more rapidly with increasing water flow rates. As indicated by Figure 4, the transition from a solid to a liquid phase for water flow rates of 1, 2, and 3 LPM takes place at the 76th minute, 66th minute, and 59th minute, respectively. The start of the PCM melting process for a discharge of 3 LPM is the fastest because the thermal energy in the TES tank is high. These results confirm the study by Chopra et al. (2020) above.

HTF Average Temperature Evolution of Each Layer

The positioning of thermocouples for the HTF varies in terms of height. The distances of thermocouples T_{11} and T_{12}, T_{13} and T_{14}, T_{15} and T_{16}, T_{17} and T_{18}, T_{19} and T_{20}, T_{21}, and T_{22} from the bottom of the tank are 21.25 cm, 17.75 cm, 14.25 cm, 10.75 cm, 7.25 cm, and 3.75 cm, respectively. Figure 5 depicts the progression of the average temperature at each HTF height for a water flow rate of 3 LPM.

The graph depicted in Figure 5 shows a rise in HTF temperature throughout the charging process. However, the temperature progression varies across different layers of the HTF. The sequence of HTF temperature

evolution from the lowest to the highest corresponds to layers at 3.75 cm, 7.25 cm, 10.75 cm, 14.25 cm, 17.75 cm, and 21.25 cm, respectively. This observation highlights that as the HTF layer elevates, so does the temperature. Majumdar and Saha (2019) suggest that the upper part of the tank contains hot water due to its lower density, while colder water, denser because of gravity's influence, occupies the bottom. This stratification of HTF layers at varying temperatures is termed thermal stratification (Chidambaram et al., 2011). Fazilati and Alemrajabi (2013) affirm that the experiment verifies the presence of visual stratification within the TES tank.

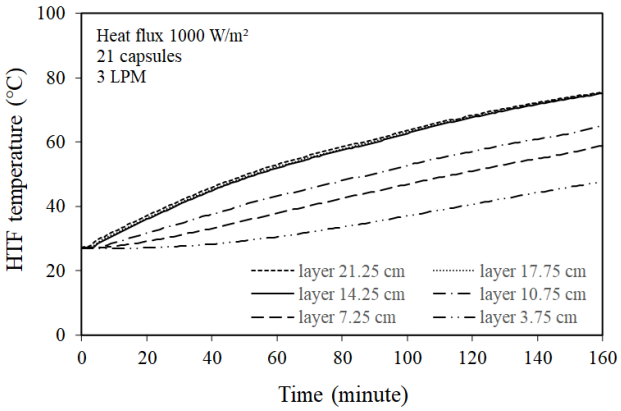

Figure 5. Evolution of average HTF temperature at a certain thermocouple height

Figure 5 also shows that the 14.25 cm, 17.75 cm, and 21.25 cm layers have close HTF temperatures. The positions of the 10.75 cm and 14.25 cm HTF thermocouples are the layers below and above the middle capsule (on the tank axis). At the same time, the water enters the tank along its central axis, directing the flow to impact the middle capsule. The collision of the water flow is suspected to be towards the top of the tank so that more hot water goes to the top of the tank. Thus, the HTF temperatures in the 14.25 cm, 17.75 cm, and 21.25 cm layers do not have a height difference because the layers are only 3.5 cm apart.

Richardson Number

The Richardson number is directly linked to the disparity in temperature between the upper and lower portions of the tanks, as outlined in Equation (1). Figure 6 illustrates the fluctuation in temperature differences over the 160-minute heating period for various water flow rates. Across all variations, there is an initial sharp rise in temperature difference upon commencing the charging process, followed by a subsequent decline and stabilization. This abrupt increase in temperature difference arises from the suboptimal mixing of hot and cold water within the tank. However, as time progresses, the mixing improves due to the influence of water flow, reducing the temperature difference between the top and bottom sections of the tank. Consequently, the rate of increase diminishes. Furthermore, Figure 6 indicates that higher water flow rates correspond to minor temperature differences. This phenomenon is attributed to heightened water mixing at higher flow rates within the tank.

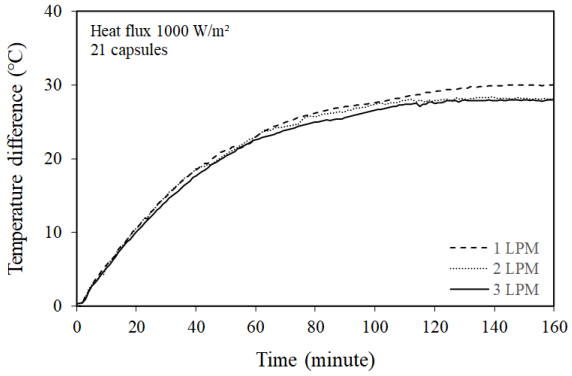

Figure 6. Evolution of HTF temperature difference between the upper and lower sections of the tank

Figure 7 illustrates the Richardson number for the three different water flow rates throughout the charging process. Over time, the Richardson number rises consistently for all flow rate variations. Equation (2) establishes a direct relationship between the average water velocity at the stratifier and the water flow rate. Meanwhile, Equation (1) reveals that the Richardson number is inversely related to the average velocity of water and directly linked to the disparity in HTF temperature between the upper and lower tanks (as depicted in Figure 6). Consequently, as the water flow rate increases, the Richardson number decreases.

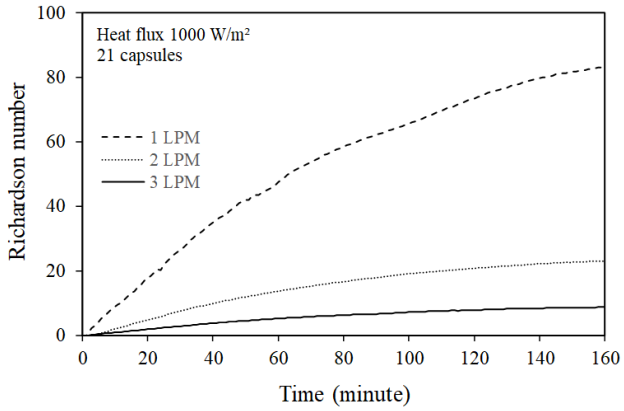

Figure 7. Evolution of Richardson number with varying water flow rate

Brown and Lai (2011) explained that thermal stratification has formed when the Richardson number equals 0.615. Meanwhile, according to (Fertahi et al., 2018), a Richardson number exceeding 1 signifies the effective thermal performance of a storage tank. Based on the findings of the preceding investigation, Figure 7 indicates the formation of thermal stratification in the TES tank across all water flow rate variations. After the charging process, the Richardson number values for water flow rates 1, 2, and 3 LPM amount to 83.32, 23.08, and 8.77, respectively. The average increment in the Richardson number value throughout charging, transitioning from a water flow rate of 3 LPM to 2 LPM, is 152.66%, while from 2 LPM to 1 LPM, it is 288.14%. A smaller water flow rate corresponds to a higher Richardson number and a swifter formation of thermal stratification. Put differently, lower water flow rates yield enhanced thermal stratification. Conversely, an increase in water flow rate intensifies the mixing of hot and cold water within the tank due to the influence of flow turbulence. This phenomenon causes the thickness of the thermocline zone to increase and the Richardson number to decrease so that thermal stratification is reduced (Wang et al., 2020).

Thermal stratification in SWH tanks is highly beneficial. It signifies the establishment of a thermal gradient across the tank's cross-section, with each layer of the HTF exhibiting a distinct temperature. This stratification offers the advantage of minimizing heat loss from the tank. Increased thermal stratification decreases the average temperature of the heat transfer fluid (HTF) within the tank, thereby minimizing thermal losses to the surroundings. This optimization enhances the efficiency of thermal energy storage. The thermal efficiency of the SWH system is determined by the proportion of valuable energy to the energy received by the collector. The effectiveness of the collector is impacted by the temperature differential between its outlet and inlet. With greater thermal stratification within the tank, the HTF temperature at the tank's outlet decreases, lowering the HTF temperature entering the collector. Consequently, this increases the valuable energy captured by the collector, resulting in improved thermal efficiency. Enhancing thermal stratification within the tank leads to improved SWH systems' thermal efficiency, as Fertahi et al. (2018) highlighted. Thermal efficiency is bolstered when there is a considerable temperature disparity between the water entering and exiting the tank, a condition ensured by thermal stratification.

The SWH system incorporating PCM capsules within the tank ensures the establishment of thermal stratification, as depicted in Figure 5. The configuration of cylindrical PCM capsules within a horizontal TES tank possesses distinctive attributes, wherein thermal energy storage is more pronounced for capsules positioned at higher levels (Nadjib et al., 2022). Variations in stored thermal energy along the tank's diameter arise due to differing temperatures of the water layers surrounding the capsules, leading to thermal stratification.

These findings align with conclusions drawn by prior researchers. Integration of PCM into SWH systems enhances thermal performance metrics such as the stratification number and thermal efficiency of TES tanks (Murali et al., 2015). Incorporating PCM capsules aids in the formation of stratification within the tank (Kumar et al., 2016). Positioning PCM near the tank's water inlet can further enhance thermal stratification (Huang et al., 2019). Given these discoveries, it would be compelling to conduct analogous investigations by altering the tank's inlet and outlet positions. In this setup, the tank inlet is at the top, whereas the outlet is at the bottom. This analysis is imperative to determine which tank inlet and outlet configuration fosters enhanced thermal stratification.

CONCLUSION

This paper presents an experimental investigation into thermal stratification in an active-type SWH system integrated with PCM within a horizontal tank. A solar simulator was utilized as the energy source for the study. The characteristics of thermal stratification were analyzed concerning variations in water flow rates using the Richardson number, and the outcomes were compared. After the 160-minute charging process, the Richardson number values for water flow rates of 1 LPM, 2 LPM, and 3 LPM were 83.32, 23.08, and 8.77, respectively. A lower water flow rate corresponded to a higher Richardson number, indicative of improved thermal stratification within the tank. The findings underscore the pivotal role of water flow rate in shaping thermal stratification. Incorporating PCM into the SWH tank sustains thermal stratification, enhancing the system's thermal efficiency. Further research can be carried out by changing the construction of the tank inlet and outlet pipes.

REFERENCES

Abokersh, M. H., Osman, M., El-Baz, O., El-Morsi, M., & Sharaf, O. (2018). Review of the phase change material (PCM) usage for solar domestic water heating systems (SDWHS). *International Journal of Energy Research*, *42*(2), 329–357. https://doi.org/10.1002/er.3765

Anisur, M. R., Mahfuz, M. H., Kibria, M. A., Saidur, R., Metselaar, I. H. S. C., & Mahlia, T. M. I. (2013). Curbing global warming with phase change materials for energy storage. *Renewable and Sustainable Energy Reviews*, *18*, 23–30. https://doi.org/10.1016/j.rser.2012.10.014

Bauer, N., Hilaire, J., Brecha, R. J., Edmonds, J., Jiang, K., Kriegler, E., Rogner, H. H., & Sferra, F. (2016). Assessing global fossil fuel availability in a scenario framework. *Energy*, *111*, 580–592. https://doi.org/10.1016/j.energy.2016.05.088

Brown, N. M., & Lai, F. C. (2011). Enhanced thermal stratification in a liquid storage tank with a porous manifold. *Solar Energy*, *85*(7), 1409–1417. https://doi.org/10.1016/j.solener.2011.03.024

Castell, A., Medrano, M., Solé, C., & Cabeza, L. F. (2010). Dimensionless numbers used to characterize stratification in water tanks for discharging at low flow rates. *Renewable Energy*, *35*(10), 2192–2199. https://doi.org/10.1016/j.renene.2010.03.020

Chandra, Y. P., & Matuska, T. (2019). Stratification analysis of domestic hot water storage tanks: A comprehensive review. *Energy and Buildings*, *187*, 110–131. https://doi.org/10.1016/j.enbuild.2019.01.052

Chidambaram, L. A., Ramana, A. S., Kamaraj, G., & Velraj, R. (2011). Review of solar cooling methods and thermal storage options. *Renewable and Sustainable Energy Reviews*, *15*(6), 3220–3228. https://doi.org/10.1016/j.rser.2011.04.018

Chopra, K., Pathak, A. K., Tyagi, V. V., Pandey, A. K., Anand, S., & Sari, A. (2020). Thermal performance of phase change material integrated heat pipe evacuated tube solar collector system: An experimental assessment. *Energy Conversion and Management*, *203*, 112205. https://doi.org/10.1016/j.enconman.2019.112205

Dehghan, A. A., & Barzegar, A. (2011). Thermal performance behavior of a domestic hot water solar storage tank during consumption operation. *Energy Conversion and Management*, *52*(1), 468–476. https://doi.org/10.1016/j.enconman.2010.06.075

Fang, Y., Niu, J., & Deng, S. (2018). Numerical analysis for maximizing effective energy storage capacity of thermal energy storage systems by enhancing heat transfer in PCM. *Energy and Buildings*, *160*, 10–18.

https://doi.org/10.1016/j.enbuild.2017.12.006

Fazilati, M. A., & Alemrajabi, A. A. (2013). Phase change material for enhancing solar water heater, an experimental approach. *Energy Conversion and Management*, *71*, 138–145. https://doi.org/10.1016/j.enconman.2013.03.034

Fertahi, S. ed D., Jamil, A., & Benbassou, A. (2018). Review on Solar Thermal Stratified Storage Tanks (STSST): Insight on stratification studies and efficiency indicators. *Solar Energy*, *176*, 126–145. https://doi.org/10.1016/j.solener.2018.10.028

Fukahori, R., Nomura, T., Zhu, C., Sheng, N., Okinaka, N., & Akiyama, T. (2016). Macro-encapsulation of metallic phase change material using cylindrical-type ceramic containers for high-temperature thermal energy storage. *Applied Energy*, *170*, 324–328. https://doi.org/10.1016/j.apenergy.2016.02.106

Huang, H., Wang, Z., Zhang, H., Dou, B., Huang, X., Liang, H., & Goula, M. A. (2019). An experimental investigation on thermal stratification characteristics with PCMs in solar water tank. *Solar Energy*, *177*, 8–21. https://doi.org/10.1016/j.solener.2018.11.004

Jamar, A., Majid, Z. A. A., Azmi, W. H., Norhafana, M., & Razak, A. A. (2016). A review of water heating system for solar energy applications. *International Communications in Heat and Mass Transfer*, *76*, 178–187. https://doi.org/10.1016/j.icheatmasstransfer.2016.05.028

Kabir, E., Kumar, P., Kumar, S., Adelodun, A. A., & Kim, K. H. (2018). Solar energy: Potential and future prospects. *Renewable and Sustainable Energy Reviews*, *82*, 894–900. https://doi.org/10.1016/j.rser.2017.09.094

Kanimozhi, B., & Bapu, B. R. R. (2012). Experimental study of thermal energy storage in solar system using PCM. *Advanced Materials Research*, *433–440*, 1027–1032. https://doi.org/10.4028/www.scientific.net/AMR.433-440.1027

Khare, S., Dell'Amico, M., Knight, C., & McGarry, S. (2013). Selection of materials for high temperature sensible energy storage. *Solar Energy Materials and Solar Cells*, *115*, 114–122. https://doi.org/10.1016/j.solmat.2013.03.009

Koželj, R., Mlakar, U., Zavrl, E., Stritih, U., & Stropnik, R. (2021). An experimental and numerical analysis of an improved thermal storage tank with encapsulated PCM for use in retrofitted buildings for heating. *Energy and Buildings*, *248*. https://doi.org/10.1016/j.enbuild.2021.111196

Kumar, G. S., Nagarajan, D., Chidambaram, L. A., Kumaresan, V., Ding, Y., & Velraj, R. (2016). Role of PCM addition on stratification behaviour in a thermal storage tank – An experimental study. *Energy*, *115*, 1168–1178. https://doi.org/10.1016/j.energy.2016.09.014

Kushwaha, P. K., Sharma, N. K., Kumar, A., & Meena, C. S. (2023). Recent Advancements in Augmentation of Solar Water Heaters Using Nanocomposites with PCM: Past, Present, and Future. *Buildings*, *13*(1), 79. https://doi.org/10.3390/buildings13010079

Majumdar, R., & Saha, S. K. (2019). Effect of varying extent of PCM capsule filling on thermal stratification performance of a storage tank. *Energy*, *178*, 1–20. https://doi.org/10.1016/j.energy.2019.04.101

Murali, G., Mayilsamy, K., & Arjunan, T. V. (2015). An experimental study of PCM-incorporated thermosyphon solar water heating system. *International Journal of Green Energy*, *12*(9), 978–986. https://doi.org/10.1080/15435075.2014.888663

Nadjib, M., Suhanan, & Waluyo, J. (2020). Experimental investigation of thermal behavior in an active type solar water heater based on phase change material using solar simulator. *AIP Conference Proceedings*, *2296*(1), 20040. https://doi.org/10.1063/5.0030475

Nadjib, M., Wahyudi, W., Anggara, F., & Irawan, Y. H. (2022). Effectiveness of capsules installation containing paraffin wax in a solar water heater. *Sinergi*, *26*(2), 229. https://doi.org/10.22441/sinergi.2022.2.012

Naveenkumar, R., Ravichandran, M., Mohanavel, V., Karthick, A., Aswin, L. S. R. L., Priyanka, S. S. H., Kumar, S. K., & Kumar, S. P. (2022). Review on phase change materials for solar energy storage applications. *Environmental Science and Pollution Research*, *29*(7), 9491–9532. https://doi.org/10.1007/s11356-021-17152-8

Nazir, H., Batool, M., Bolivar Osorio, F. J., Isaza-Ruiz, M., Xu, X., Vignarooban, K., Phelan, P., Inamuddin, & Kannan, A. M. (2019). Recent developments in phase change materials for energy storage applications: A review. *International Journal of Heat and Mass Transfer*, *129*, 491–523.

https://doi.org/10.1016/j.ijheatmasstransfer.2018.09.126

Ostadzadeh, E., Elshorbagy, A., Tuninetti, M., Laio, F., & Abdelkader, A. (2023). Who will dominate the global fossil fuel trade? *Economic Systems Research*, *35*(3), 354–375. https://doi.org/10.1080/09535314.2023.2174002

Patel, A., & Namjoshi, S. (2018). Phase Change Material Based Solar Water Heater. *International Journal of Engineering and Science Invention*, *5*(8), 31–34.

Pinel, P., Cruickshank, C. A., Beausoleil-Morrison, I., & Wills, A. (2011). A review of available methods for seasonal storage of solar thermal energy in residential applications. *Renewable and Sustainable Energy Reviews*, *15*(7), 3341–3359. https://doi.org/10.1016/j.rser.2011.04.013

Rubitherm Technologies GmbH. (2020). *Technisches Datenblatt RT55*. www.rubitherm.com

Salunkhe, P. B., & Shembekar, P. S. (2012). A review on effect of phase change material encapsulation on the thermal performance of a system. *Renewable and Sustainable Energy Reviews*, *16*(8), 5603–5616. https://doi.org/10.1016/j.rser.2012.05.037

Shabtay, Y. L., & Black, J. R. H. (2014). Compact hot water storage systems combining copper tube with high conductivity graphite and phase change materials. *Energy Procedia*, *48*, 423–430. https://doi.org/10.1016/j.egypro.2014.02.049

Shahsavari, A., & Akbari, M. (2018). Potential of solar energy in developing countries for reducing energy-related emissions. *Renewable and Sustainable Energy Reviews*, *90*, 275–291. https://doi.org/10.1016/j.rser.2018.03.065

Singh, S., Anand, A., Shukla, A., & Sharma, A. (2020). Technical, financial, and environmental feasibility of solar water heater for residential, commercial, and industrial application: A theoretical approach. *Materials Science for Energy Technologies*, *3*, 648–671. https://doi.org/10.1016/j.mset.2020.07.001

Sobhansarbandi, S., Martinez, P. M., Papadimitratos, A., Zakhidov, A., & Hassanipour, F. (2017). Solar thermal collector with multifunctional absorber layers. *American Society of Mechanical Engineers, Power Division (Publication) POWER*, *2*, 342–350. https://doi.org/10.1115/POWER-ICOPE2017-3545

Uctug, F. G., & Azapagic, A. (2018). Life cycle environmental impacts of domestic solar water heaters in Turkey: The effect of different climatic regions. *Science of the Total Environment*, *622–623*, 1202–1216. https://doi.org/10.1016/j.scitotenv.2017.12.057

Wang, Z., Zhang, H., Dou, B., Zhang, G., Wu, W., & Zhou, L. (2020). An experimental study for the enhancement of stratification in heat-storage tank by equalizer and PCM module. *Journal of Energy Storage*, *27*, 101010. https://doi.org/10.1016/j.est.2019.101010

World Energy Council. (2013). World Energy Resources: 2013 survey. In *World Energy Council* (p. 11). http://www.worldenergy.org

Wu, W., Dai, S., Liu, Z., Dou, Y., Hua, J., Li, M., Wang, X., & Wang, X. (2018). Experimental study on the performance of a novel solar water heating system with and without PCM. *Solar Energy*, *171*, 604–612. https://doi.org/10.1016/j.solener.2018.07.005

Xiao, X., & Zhang, P. (2015). Numerical and experimental study of heat transfer characteristics of a shell-tube latent heat storage system: Part I - Charging process. *Energy*, *79*(C), 337–350. https://doi.org/10.1016/j.energy.2014.11.020